ORIGINAL ARTICLE

Silicon Vacancy Color Centers in 6H-SiC Fabricated by Femtosecond Laser Direct Writing

Zhanqi Zhou[1] · Zongwei Xu[1] · Ying Song[1] · Changkun Shi[1] · Kun Zhang[1] · Bing Dong[1]

Abstract

As a single photon source, silicon vacancy (V_{Si}) centers in wide bandgap semiconductor silicon carbide (SiC) are expected to be used in quantum technology as spin qubits to participate in quantum sensing and quantum computing. Simultaneously, the new direct femtosecond (fs) laser writing technology has been successfully applied to preparing V_{Si}s in SiC. In this study, 6H-SiC, which has been less studied, was used as the processed material. V_{Si} center arrays were formed on the 6H-SiC surface using a 1030-nm-wavelength fs pulsed laser. The surface was characterized by white light microscopy, atomic force microscopy, and confocal photoluminescence (PL)/Raman spectrometry. The effect of fs laser energy, vector polarization, pulse number, and repetition rate on 6H-SiC V_{Si} defect preparation was analyzed by measuring the V_{Si} PL signal at 785-nm laser excitation. The results show that fs laser energy and pulse number greatly influence the preparation of the color center, which plays a key role in optimizing the yield of V_{Si}s prepared by fs laser nanomachining.

Highlights

1. Color centers arrays of silicon vacancy were fabricated on 6H-SiC surface by fs laser.
2. AFM and PL/ Raman spectrometer were used to characterize the morphology of the processing a rea and the forma tion of V_{Si}.

3. The influence of laser parameters i n the process of color center preparation by fs laser is studied, and the laser energy and las er pulse number are the main influencing factors.

1 Introduction

Silicon carbide (SiC), as a new third-generation wide-band-gap semiconductor material, has the advantages of high transparency, high band gap width, high saturation drift speed, high thermal conductivity, radiation resistance, etc. [1–4]. Currently, the commonly used SiC crystal types are 3C-SiC, 4H-SiC, and 6H-SiC. SiC crystals contain various color centers, among which silicon vacancy (V_{Si}) color centers are mostly used. The single V_{Si} color center is a good single photon source with advantages such as long spin coherence time and easy integration and can also be used as a spin qubit at room temperature [5–8]. Therefore, it is widely used in quantum communication and quantum sensing [9–13].

At present, the technologies for preparing V_{Si} centers in high-purity SiC are mainly focused electron beam irradiation [14], neutron beam irradiation [15], proton beam irradiation [16], and ion beam irradiation [17, 18]. After processing, the color center is generated by annealing treatment [10]. However, these methods can induce much residual lattice damage during processing, which reduces the spin and optical coherence characteristics of V_{Si} color centers [19]. Recently, the research on preparing color centers in

✉ Zongwei Xu
zongweixu@tju.edu.cn

1 State Key Laboratory of Precision Measuring Technology and Instruments, Laboratory of Micro/Nano Manufacturing Technology, Tianjin University, Tianjin 300072, China

wide-gap semiconductor materials based on femtosecond (fs) laser writing has attracted wide attention [20–22]. At present, the method for fabricating nitrogen vacancy centers near a diamond surface by fs laser writing technology is relatively mature [23–26], and the technology for fabricating silicon carbide V_{Si} has been gradually improving. Castelletto et al. created local photoluminescence (PL) emission regions in 4H-SiC and 6H-SiC using direct fs laser writing technology and achieved specific V_{Si} center emission in the range of 850–950 nm [27]. Chen et al. created single V_{Si} centers in 4H-SiC using laser writing without any post-annealing process and discussed the mechanism of the laser writing process [28]. Castelletto et al. prepared numerous V_{Si} defect arrays in 4H-SiC and found that the number of color centers formed exhibited power-law scaling with the laser processing energy, indicating that the color centers were created by photoinduced ionization [29, 30]. At present, the creation of 4H-SiC color centers technology is a relatively mature research topic, but the creation of V_{Si} by the fs laser writing of 6H-SiC is rarely researched.

In this work, we applied fs laser writing to create color centers in 6H-SiC. Atomic force microscopy (AFM) was used to characterize the damage morphology in the machining area. Combined with confocal PL/Raman spectroscopy, the PL characteristics of the fs laser writing region were characterized, and color center preparation was analyzed. Additionally, the effects of fs laser energy, polarization, pulse number, and repetition rate on the V_{Si} defects of 6H-SiC were studied. The results can guide the fabrication of devices containing V_{Si} by fs laser.

2 Experimental Work

The host material used in this study was a double-sided polished *N*-type 6H-SiC substrate from PAM-XIAMEN, with a $4° \pm 0.5°$ off-axis and a bias of <11–20>. A schematic of the fs laser writing device is shown in Fig. 1. A fiber fs laser with a 1030-nm wavelength, 361-fs pulse duration, and a repetition rate of 100/200/500 kHz were used. The magnification of the objective lens was 50×, and the numerical aperture was NA = 0.42. The percentage of laser output power can be controlled through the laser software, and one can adjust the first half-wavelength plate (HWP) in the laser system to obtain the required laser energy. A high-precision mechanical platform was used for the three-dimensional movement of the sample, and the displacement accuracy was 0.5 nm.

First, piranha solution (concentrated sulfuric acid: hydrogen peroxide = 3:1) was used to clean the SiC sample to remove the organic contaminants on the surface, and cleaning it with acetone, ethanol, and deionized water in an ultrasonic bath obtained the surface-clean SiC sample.
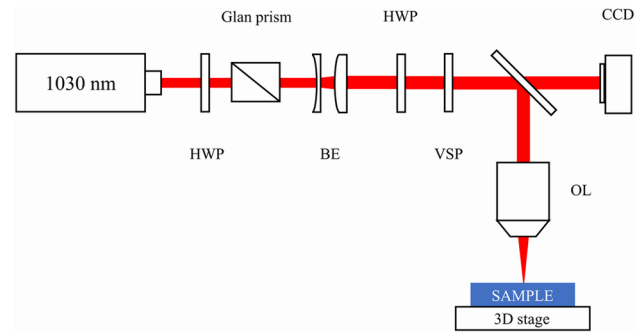
Fig. 1 Schematic of the fs laser writing device, comprising a 100/200/500-kHz 1030-nm laser, half-wavelength plate (HWP), Glan prism, beam expander (BE), variable spiral plate (VSP), and objective lens (OL)

Table 1 Details of the laser-written regions

Label	Energy (nJ)	Repetition rate (kHz)	Pulse number	Polarization
1	860–4300	100	1	Linearly polarized
2	86–4300	100	1	Azimuthally polarized
3	86–4300	100	5	Linearly polarized
4	86–4300	200	5	Linearly polarized

A 1030-nm laser was used to write four-point arrays, with a pulsed laser at each write position and a 10-μm interval between each point. The laser was focused on the surface of the SiC sample, and the laser energy of the first group was 860–4300 nJ. To study the effect of laser energy over a wider range, the laser energies of the other three groups ranged from 86 to 4300 nJ. 6H-SiC was processed using an fs laser with a different laser polarization, pulse number, and repetition rate, and the vacancy changes were compared after processing. The processing parameters are shown in Table 1. Each set of parameters was repeated ten times to verify the reproducibility of the processing results.

To obtain the photoluminescence results of the laser writing points, PL and Raman spectra were measured using a confocal microscope (Horiba XploRA PLUS and iHR550) in a backscattering geometric configuration at room temperature. The magnification of the objective lens was 100×, the numerical aperture was NA = 0.9, and the grating was 600 g/mm. The Raman characteristic peaks of the 6H-SiC laser writing damage region were measured using a 532-nm laser to judge the damage degree of the SiC crystals, including E2 (low), E2 (high), and LOPC. Since 770 nm is the optimal excitation wavelength of V_{Si} PL signals at room temperature [31], a 785-nm laser was used to test the PL signals of V_{Si}s in the 6H-SiC laser writing region to obtain the center point spectrum of the test region, the two-dimensional spectrum of the sample surface, and depth spectrum information. At the

same time, an optical microscopy and AFM (Bruker Multi-Mode8) were used to characterize the surface morphology of the laser writing processing area.

## 3 Results and Discussion

3.1 Surface Morphology

After being cleaned, the 6H-SiC sample was characterized, and the optical image of the laser writing area on its surface is shown in Fig. 2. There were four groups of processing areas, and the laser processing parameters of each group are shown in Table 1. Under the four groups of different processing parameters, the morphology of the laser write zone has obvious differences and shows good repeatability under the same parameters.

To further determine the morphological details of the damaged area, AFM was used to test the morphological characteristics of the laser writing surface, as shown in Fig. 3. Figure 3a–e shows the AFM test results of five laser writing points with a laser energy of 860–3440 nJ under the first set of processing parameters. The depth and width of the fs laser-written region under the AFM test are shown in Table 2. With increasing laser energy, the width of the processing points gradually increased from 4 to 6.4 μm. At the

Fig. 2 Optical micrograph of the laser writing on the 6H-SiC surface under 50× objective lens. **a–b** The four processing areas generated by processing parameters from groups 1–4

same time, the ablation depth showed a trend of increasing first and then decreasing and formed a bulge with the center of the processing area under high energy. The 2D/3D images in Fig. 3a show that raised particles with smaller diameters were in the pit at the center of the processing point, and a circular expansion structure with a height of 20 nm existed at the edge of the laser writing point. The particles in the center were considered the gasification of materials in the irradiation center area influenced by a Gaussian distribution of laser energy, and some of the gasification materials were recondensed into convex structures. The annular region at the edge was the expulsion of the melt caused by the recoil pressure, while the outer part forms an amorphous layer at lower energy, leading to an expansion of the material. With an increase in laser energy to 1433 nJ, the material gasification degree in the central area was strengthened, and the outward diffusion impact force of the plasma current increased, which gradually promoted a spread of gasification material, increasing the ablation depth and reducing the roughness of the ablation area, as shown in Fig. 3b and c. This increase in laser energy also increased the melt discharged from the edge region and increased the amorphous layer. As shown in Fig. 3d and e, as the laser energy continued to increase, the molten layer in the central region increased, and the width of the heat-affected zone increased. The redeposition under the influence of recoil force could not be pushed out to the surrounding area because of the laser single-pulse writing, which led to a reduction of the central ablation depth [32]. The poor symmetry of each processing point was due to the imperfect adjustment of the optical path and the small NA of the objective lens [33].

3.2 Raman Spectral Characterization

To determine the damage to the SiC lattice caused by laser writing, Raman spectroscopy was applied to the laser writing points. We observed in the pristine and damaged parts of the sample the transverse optic (TO) and longitudinal optic peaks associated with 6H-SiC Raman vibrational modes, which are of greatest concern and are sensitive to the crystal quality [27]. The Raman spectra of 6H-SiC samples in the pristine areas were compared with those in different laser writing areas. During the test, a 532-nm laser was used to excite the Raman spectra of the first machining region (single pulse, 100-kHz repetition rate), and the results are shown in Fig. 4 (a low-pressure mercury lamp was used for calibration to ensure the accuracy of the Raman peak wave numbers). Identical Raman characteristic peaks were observed in the spectra of the laser writing area and the pristine area. E_2 (low) and E_2 (high) peaks are two TO peaks of 6H-SiC. Additionally, the LOPC peak is longitudinal optic phonon–plasmon coupled with 6H-SiC. The strength of these three Raman peaks represents the content of SiC in
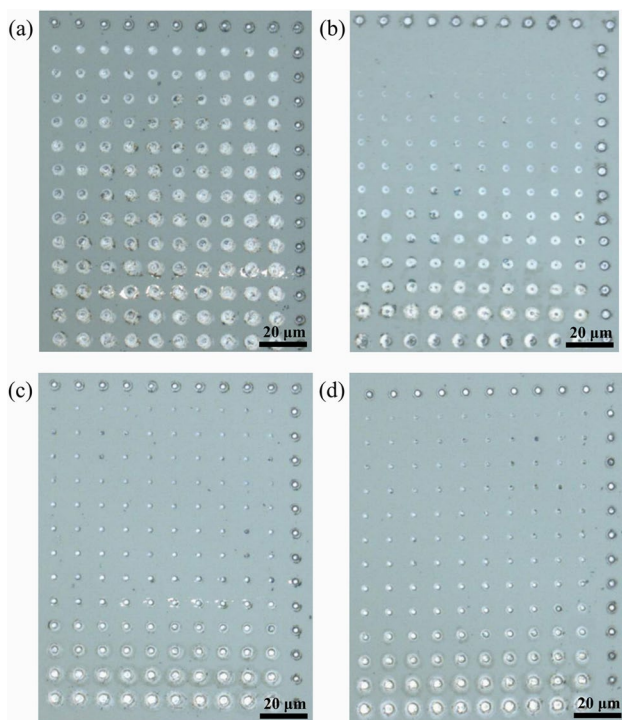
Fig. 3 First set of AFM images of the laser writing area. **a**–**e** 2D/3D ▶ surface morphologies at five energies and profiles of dotted lines

the test region. If the SiC lattice is damaged, the strength of these peaks will decrease. Therefore, the lattice damage to SiC can be obtained by comparing these three Raman peaks of SiC before and after fs laser processing.

Figure 5 shows the variations in Raman peak intensity and frequency shift under different machining powers, which have similar trends. With increasing laser processing energy, the peak intensity decreased. At the same time, the higher the laser energy was, the weaker the decreasing trend of peak intensity. The Raman peaks underwent an obvious frequency shift, reflecting a tensile stress change in the machining area under laser irradiation. This change was due to the increased damage to the 6H-SiC crystalline structure in the machined region, as well as the scattering effects due to surface melting.

3.3 PL Characterization

3.3.1 Effect of Laser Energy

Similar to the presence of two nonequivalent V_{Si} defects in 4H-SiC, three nonequivalent V_{Si} defects exist in 6H-SiC, namely, V1, V2, and V3 centers. Their zero phonon lines are 867, 889, and 909 nm at 5.5 K, respectively [34]. At room temperature, the fluorescence peak of the V_{Si}s is broadened to the range of 850–950 nm [27]. To study the effect of fs laser parameters on V_{Si} preparation and obtain higher PL excitation efficiency of V_{Si}s, the PL spectra of V_{Si} defects in the 6H-SiC processing region were measured using a 785-nm laser at room temperature. The test points were focused on the sample surface to test the first group of processing areas (single pulse, 100-kHz repetition rate), and the PL spectra test results are shown in Fig. 6. The written region with a laser energy of 860 nJ had basically the same PL spectra as the original region, and no new peaks appeared, so no additional V_{Si} was considered to have been generated. When the laser energy increased to 1147 nJ, the V_{Si} signal region (i.e., the range of 850–950 nm) showed obvious enhancement. The laser processing energy was considered to have reached the threshold of V_{Si} generation in the range of 860–1147 nJ. The V_{Si} maximum PL signal appeared at 2866 nJ energy. Additionally, the energy continued to increase, and the PL signal strength decreased. These results indicated that V_{Si}s were successfully prepared when the laser energy was increased to the threshold of 6H-SiC V_{Si} processing under the condition of other processing parameters being fixed. With increasing energy, the V_{Si} density in the laser writing region increased. However, the increase in laser energy had an upper limit, which was considered to destroy the prepared V_{Si}s. For example, when the laser energy increased to 3440 nJ, the PL signal was weakened.
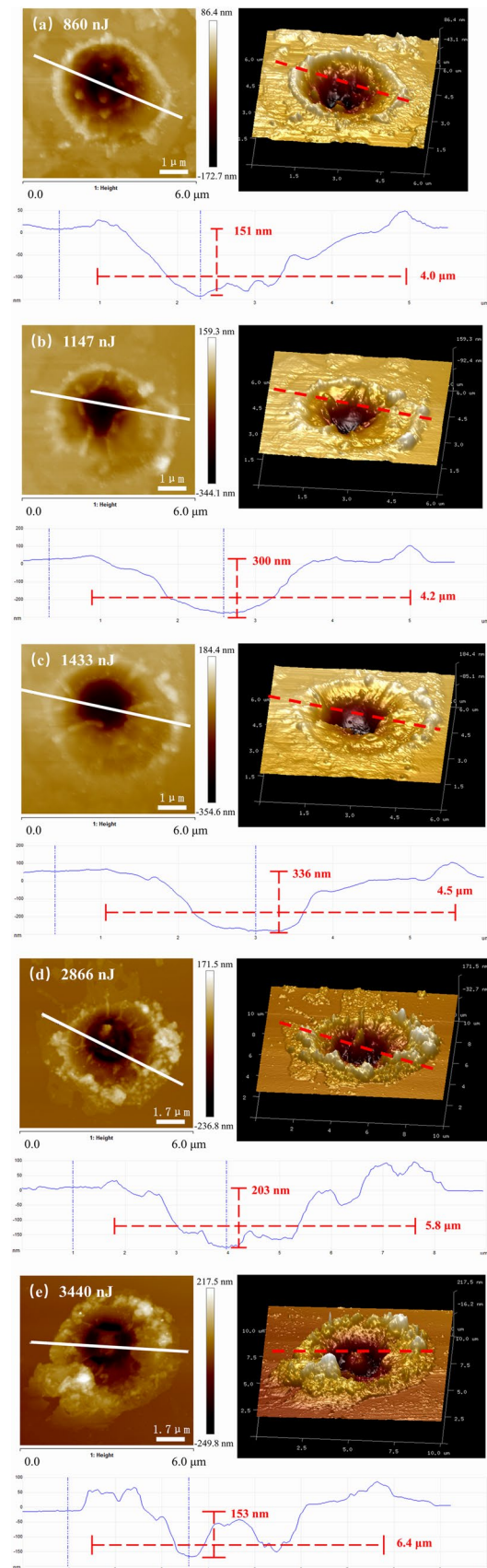
Table 2 Depth and width of the laser-written regions according to the AFM results

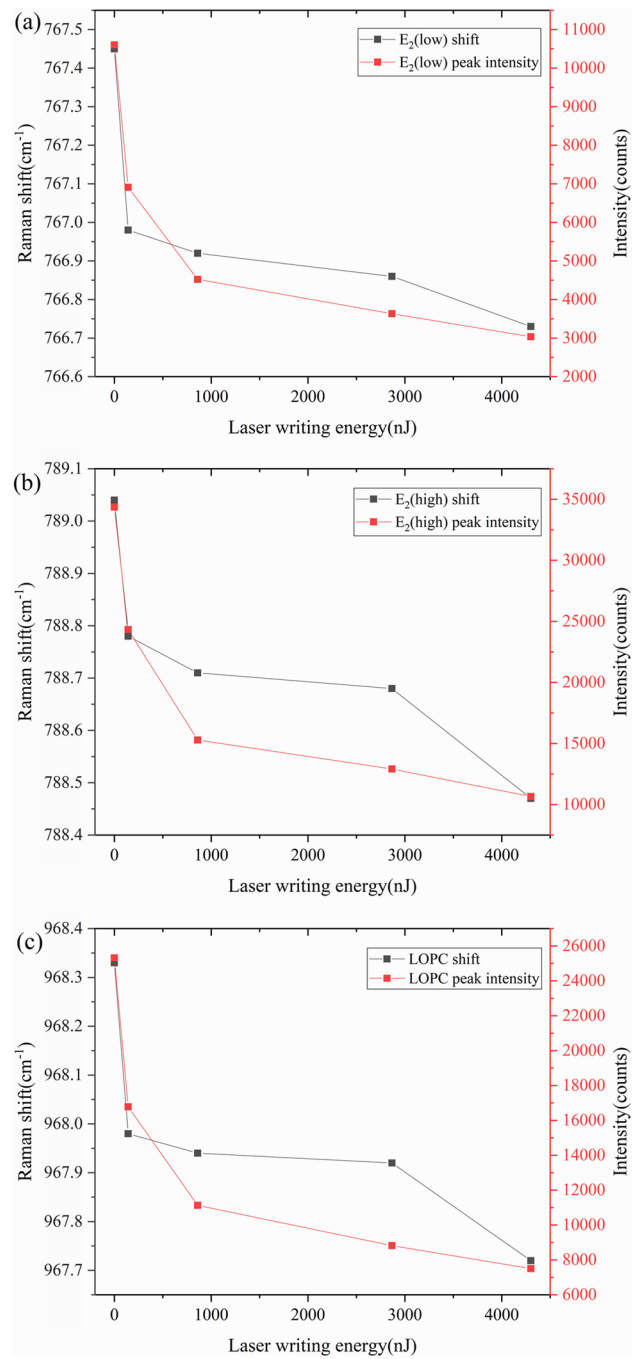| Label	Energy (nJ)	Max. depth (nm)	Width (μm)
1	860	151	4.0
2	1147	300	4.2
3	1433	336	4.5
4	2866	203	5.8
5	3440	153	6.4
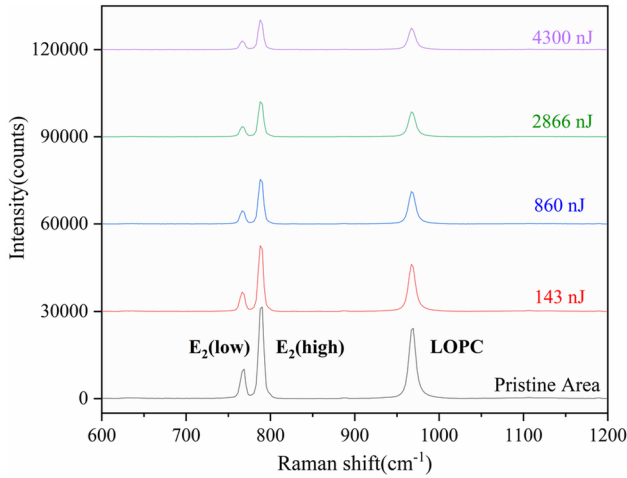
Fig. 4 Raman spectra of an unmodified 6H-SiC surface and from 143 to 4300 nJ laser writing spots in the first set of machining regions excited by a 532-nm laser

Fig. 5 Intensity and frequency shift of the 6H-SiC Raman characteristic peaks: **a** E_2 (low), **b** E_2 (high), and **c** LOPC

Therefore, a laser writing energy of 2866 nJ in this processing environment will obtain higher V_{Si} production.

The production of color centers in SiC may be attributed to the effect of multiphoton ionization (MPI) and tunneling ionization (Zener breakdown) caused by a longer manufacturing wavelength, and the V_{Si} ensemble is generated at higher laser energy [27]. The dominant mechanism in the nonlinear absorption regime for free-electron generation is typically delineated by the Keldysh parameter, which is given by Eq. (1.1), where ω is the laser angular frequency, e is the electron charge, m is the reduced mass, n is the medium refractive index, ε_0 is the permittivity of free space, E_g is the 6H-SiC band gap width, and I is the laser irradiance at the focal plane. The threshold intensity of V_{Si} creation in the intermediate region between MPI and tunneling ionization can be derived, as shown in Eq. (1.2).
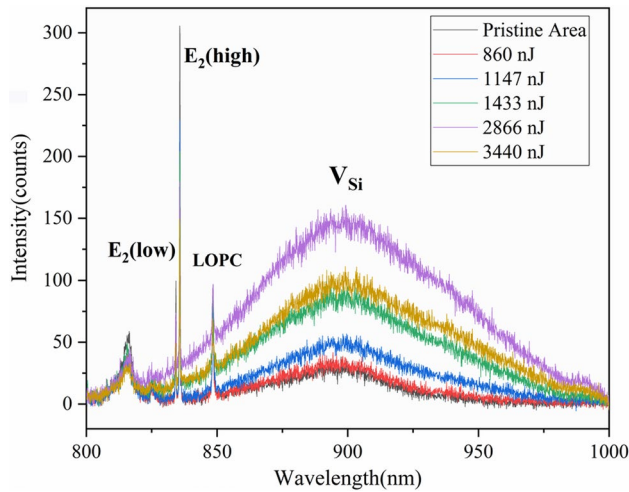
$$\gamma = \frac{\omega}{e}\sqrt{\frac{mcn\varepsilon_0 E_g}{2I}} \tag{1.1}$$

$$I\text{th} = \frac{mcn\varepsilon_0 E_g \omega^2}{(1.5 \times e)^2} \tag{1.2}$$

The threshold value $I \approx 1004.5$ nJ is calculated under the existing conditions considering only the influence of nonlinear absorption and is near the laser energy of the first group of processing areas when the V_{Si} signal is generated.

**Fig. 6** PL spectra of the first processing region of 6H-SiC excited by a 785-nm laser

Next, a 785-nm laser was used to focus on the SiC sample surface, and 2D PL signal mapping was performed at each processing point. The test results are shown in Fig. 7. Figure 7a–e shows similar results to the point test. With increasing laser energy, the V_{Si} PL signal at the machining center point was enhanced, and the PL signal enhancement area was expanded from 3.3 to 6.2 μm. When the energy was further increased to 3440 nJ, the V_{Si} generation area continued to increase to 6.6 μm, but the PL signal intensity at the machining center decreased. The results showed that because the laser energy was distributed in Gaussian space, V_{Si}s were generated in the machining periphery region under the low-energy laser and were partially destroyed in the machining center region under the high-energy laser. Figure 7f shows the 2D depth mapping result of the processing point when the laser energy was 2866 nJ. Additionally, the test results showed that the PL signal in the central area was strong, particularly at a depth of 0 μm, and the V_{Si} signal basically disappeared at a depth of 0.9 μm. The V_{Si} signal depth was deeper than the AFM test depth, and the transverse diffusion in the material may have been caused by the damage diffusion caused by the laser shock wave and thermal diffusion under the action of the fs laser. The PL signal had 2D transverse mapping results that showed a horseshoe shape and a longitudinal mapping result that showed an inclined cone, which was considered to be caused by an imperfect focus during laser processing and sample translation during the test.

Figure 8 superposes the AFM test results of 2866 nJ and 3440 nJ laser processing energies and their 2D mapping results, showing that the central PL signal enhancement area was basically consistent with the laser ablation area. The widening of the V_{Si} signal region compared with the ablation pit region also confirmed the analysis of Fig. 7f.
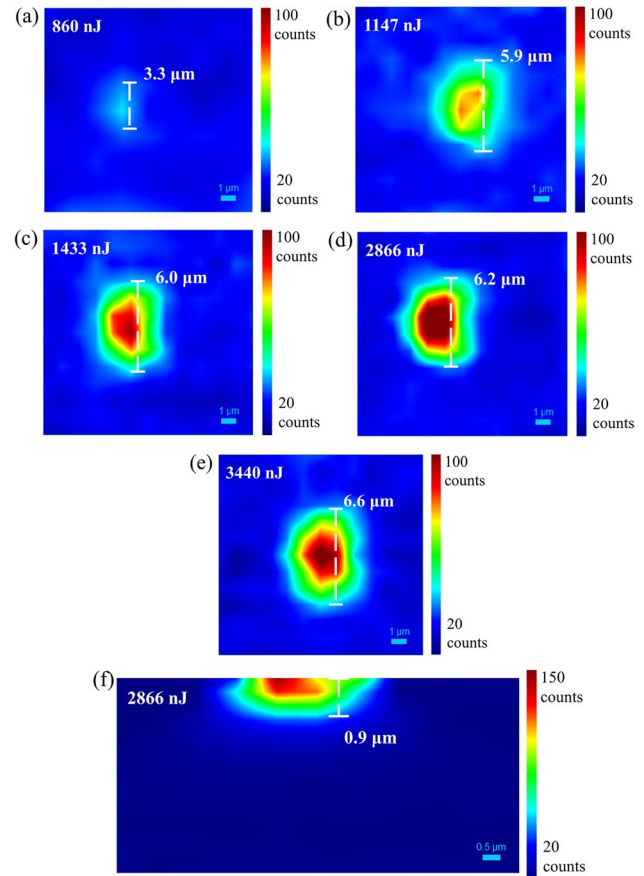
Fig. 7 2D PL mapping of V_{Si} excited by the 785-nm laser when focusing on the sample surface: **a–e** surface PL mapping and **f** depth PL mapping

At the same time, the amorphous layer near the ablation pit had no enhanced signal, indicating that no V_{Si} formation occurred in the SiC amorphous layer.
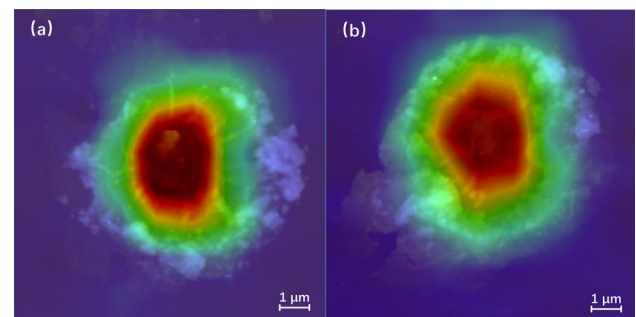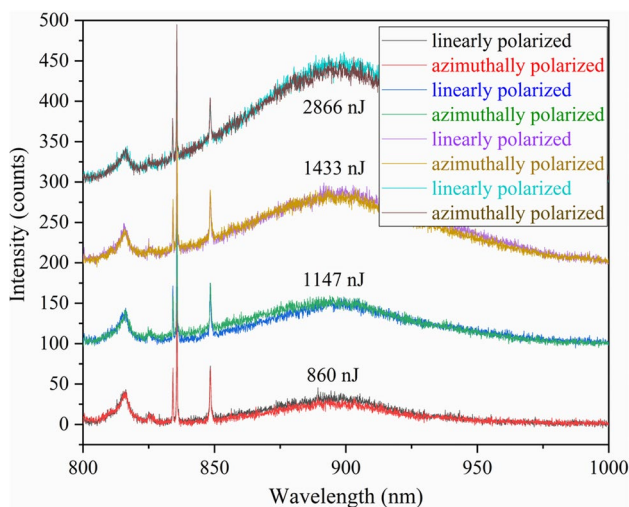

Fig. 8 Overlay of the AFM test results and 2D PL mapping of fs laser writing on SiC: **a** laser energy of 2866 nJ and **b** laser energy of 3440 nJ
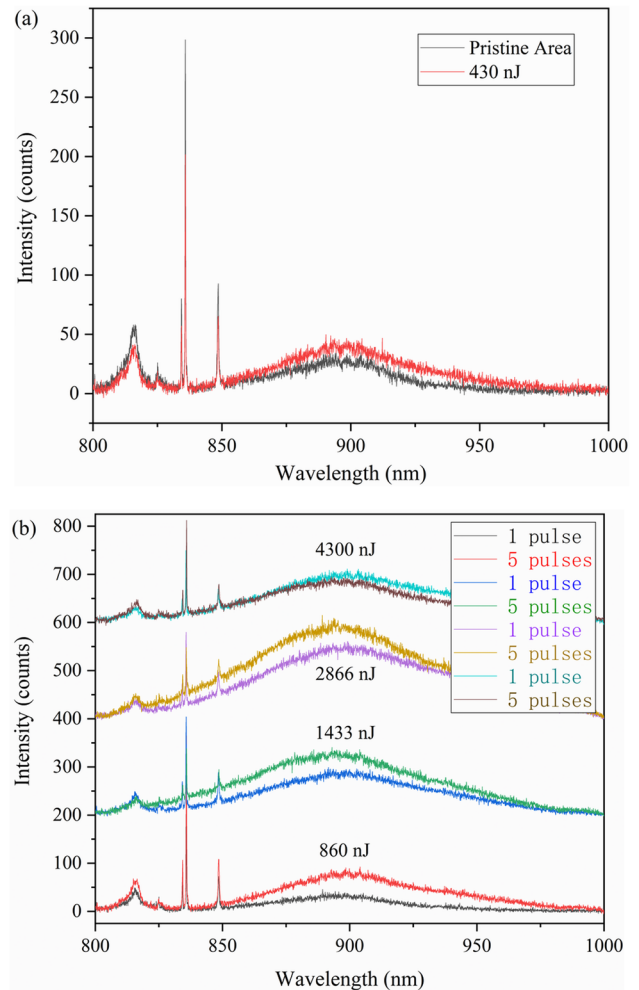
3.3.2 Effect of Laser Polarization

An fs laser with a vector light field can produce micro/nano-structures affected by vector polarization in the laser action region [35–37]. However, the influence of fs vectorial optical field micro/nanoprocessing on color center preparation is rarely studied. The second group of processing areas (single pulse, 100-kHz repetition rate, azimuthal polarization) was tested and compared to the first group regarding PL signals to explore the influence of vector optical field on color center preparation. The results are shown in Fig. 9. This figure shows that their PL signals were basically identical at different irradiation energies, so the fs laser vector polarization did not affect the V_{Si} processing results of 6H-SiC. Therefore, the effect of laser vector polarization was neglected in subsequent experiments.

3.3.3 Effect of Laser Pulse Number and Repetition Rate

First, the influence of laser pulse number was studied. The third group of processing regions (five pulses, 100-kHz repetition rate) was tested and compared to the first group regarding the PL signals. The results are shown in Fig. 10. Figure 10a shows that with an increase in the number of laser pulses, the laser energy threshold for preparing V_{Si} by the laser irradiation of 6H-SiC decreased from approximately 1147 nJ to approximately 430 nJ. This result agreed with Eq. (1.2) regarding the influence trend caused by pulse number. Figure 10b shows that when the laser energy was 860, 1433, and 2866 nJ, the V_{Si} PL signals in the irradiation area were considerably enhanced with increasing pulse number. When the laser energy was 4300 nJ, the V_{Si} signal under five-pulse processing was substantially weakened and

Fig. 10 a Minimum laser energy required for V_{Si} preparation with five laser pulses. **b** Comparison between the PL spectra of the first and third processing regions of 6H-SiC excited by a 785 nm laser

Fig. 9 Comparison of PL spectra between the first and second processing regions of 6H-SiC excited by a 785-nm laser

was slightly lower than the result of single-pulse processing. The V_{Si} damage is considered more severe under the combined action of high energy and high pulse number. This result indicates that the pulse number and energy should be increased in a certain range to reduce the amorphous damage and promote V_{Si} formation.

Second, the influence of laser repetition rate was studied. The fourth group of processing regions (five pulses, 20-kHz repetition rate) was tested, and the PL signals of the first group were compared. Figure 11 shows the results. As shown in Fig. 11, under the premise of constant laser energy and pulse number, when the laser repetition rate increased from 100 to 200 kHz, the V_{Si} fluorescence peak signal obtained by irradiated 6H-SiC increased slightly. To verify that increasing the repetition rate promotes V_{Si} generation slightly, the processing results at a 500-kHz repetition rate were compared. The results show that the PL intensity of silicon vacancies increased slightly with increasing laser
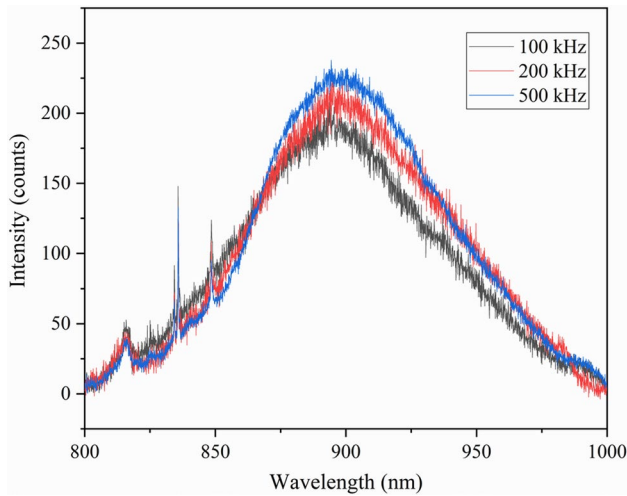
Fig. 11 Comparison of PL spectra between the third and fourth processing regions of 6H-SiC excited by a 785-nm laser. Processing results of a 2866-nJ laser at 100/200/500-kHz repetition rates

Table 3 Effect of pulse number and repetition rate on the PL intensity of V_{Si} at 2866-nJ laser energy

Pulse number	PL intensity (counts)		
	Repetition rate of 100 kHz	Repetition rate of 200 kHz	Repetition rate of 500 kHz
2	166	171	184
5	208	215	237
8	225	234	261
10	226	228	252

repetition rate, reaching a peak at 500 kHz under the present conditions. This result indicated that under the same conditions of other processing parameters, the laser repetition rate increased, which reduced the interval between two pulses and enhanced the accumulation of laser beams, promoting the generation of V_{Si}.

Additionally, to further obtain the influence of the pulse number and repetition rate on the generation of V_{Si}, 12 processing results of 2–10 pulses and a repetition rate of 100–500 kHz were analyzed (the laser energy was 2866 nJ). Their maximum PL intensity is shown in Table 3. The PL intensity slightly increased with the increase in the repetition rate under the same pulse, and the influence amplitude increased with the pulse number. The PL intensity reached its maximum when the repetition rate was 500 kHz. When the pulse number increased from 2 to 8, the PL intensity gradually increased, and when the pulse number further increased to 10, the PL intensity did not change substantially and then slightly decreased, indicating that a laser

pulse number of 8 and a repetition rate of 500 kHz were the best parameters for preparing V_{Si}.

4 Conclusions

In this study, the effect of 6H-SiC written by the different processing parameters of an fs laser on V_{Si} generation was investigated, and the test results were characterized by Raman/PL spectroscopy at 293 K. The presence of a PL peak at 900 nm detected by a 785 nm laser at normal temperature proves that V_{Si} color centers can be fabricated in 6H-SiC by direct fs laser writing technology. The formation of V_{Si} in the irradiated area is affected by laser processing parameters. By increasing the laser energy and laser pulse number in a certain range, the irradiation area can absorb more photon energy, and the accumulation of multi-pulse laser beams can increase the number of silicon vacancies generated in the irradiation area. However, high laser energy/pulse number increases the damage to the 6H-SiC machining position and destroys the generated V_{Si}s. According to the PL spectra on the surface and depth of 6H-SiC in the irradiated area, the spatial distribution of V_{Si}s in the laser writing area was obtained by comparing the surface morphology tested by AFM. The PL signal is the strongest at the laser focus and gradually weakens near the processing point, indicating that the V_{Si} yield is the highest at the center. Under the same processing parameters, the PL intensities of V_{Si}s prepared by a laser with and without a vector light field do not differ. Under the condition of constant laser energy and pulse number, increasing the laser repetition rate promotes V_{Si} generation slightly, and the promotion effect increases with the pulse number. The above results indicate that an appropriate fs laser energy and pulse number are the key to enhancing the 6H-SiC color center signal.

Author Contributions ZZ: Conceptualization, Methodology, Data collection, Analysis, Writing—original draft. ZX: Supervision, Funding acquisition, Project support. YS: Material preparation. CS: Writing—review and editing. KZh: Investigation. BD: Investigation.

Availability of Data and Materials The authors declare that all data supporting the findings of this study are available within the article.

Declarations

Competing interests The authors have no conflicts of interest to declare that are relevant to the content of this article.

References

1. Sugawara Y (2003) Recent progress in SiC power device developments and application studies. In: Proceedings of the IEEE international symposium on power semiconductor devices and ICS. https://doi.org/10.1109/ISPSD.2003.1225220

2. Wang FF, Zhang Z (2016) Overview of silicon carbide technology: device, converter, system, and application. CPSS Trans Power Electron Appl 1:13–32. https://doi.org/10.24295/CPSSTPEA.2016.00003

3. She X, Huang AQ, Lucia O, Ozpineci B (2017) Review of silicon carbide power devices and their applications. IEEE Trans Ind Electron 64:8193–8205. https://doi.org/10.1109/TIE.2017.2652401

4. Millan J, Godignon P, Tournier D (2004) Recent developments in SiC power devices and related technology. In: Proceedings of the international conference on microelectronics. https://doi.org/10.1109/ICMEL.2004.1314551

5. Atatüre M, Englund D, Vamivakas N et al (2018) Material platforms for spin-based photonic quantum technologies. Nat Rev Mater 3:38–51. https://doi.org/10.1038/s41578-018-0008-9

6. Koehl WF, Buckley BB, Heremans FJ et al (2011) Room temperature coherent control of defect spin qubits in silicon carbide. Nature 479:84–87. https://doi.org/10.1038/nature10562

7. Yan FF, Yi AL, Wang JF et al (2020) Room-temperature coherent control of implanted defect spins in silicon carbide. NPJ Quantum Inf 6:1–6. https://doi.org/10.1038/s41534-020-0270-8

8. Chen D, Gao W (2019) Quantum light sources from semiconductor. J Semicond 40:7–10. https://doi.org/10.1088/1674-4926/40/7/070301

9. Awschalom DD et al (2018) Quantum technologies with optically interfaced solid-state spins. Nat Photonics 12:516–527. https://doi.org/10.1038/s41566-018-0232-2

10. Castelletto S, Boretti A (2020) Silicon carbide color centers for quantum applications. J Phys Photonics 2:022001. https://doi.org/10.1088/2515-7647/ab77a2

11. Christle DJ, Falk AL et al (2015) Isolated electron spins in silicon carbide with millisecond coherence times. Nat Mater 14:160–163. https://doi.org/10.1038/nmat4144

12. Widmann M, Lee S-Y et al (2015) Coherent control of single spins in silicon carbide at room temperature. Nat Mater 14:164–168. https://doi.org/10.1038/nmat4145

13. Son NT, Anderson CP, Bourassa A et al (2020) Developing silicon carbide for quantum spintronics. Appl Phys Lett 116:190501. https://doi.org/10.1063/5.0004454

14. Castelletto S, Johnson BC, Ivády V et al (2014) A silicon carbide room-temperature single-photon source. Nat Mater 13:151–156. https://doi.org/10.1038/nmat3806

15. Fuchs F, Stender B, Trupke M et al (2015) Engineering near-infrared single-photon emitters with optically active spins in ultrapure silicon carbide. Nat Commun 6:7578. https://doi.org/10.1038/ncomms8578

16. Kraus H, Simin D, Kasper C et al (2017) Three-dimensional proton beam writing of optically active coherent vacancy spins in silicon carbide. Nano Lett 17:2865–2870. https://doi.org/10.1021/acs.nanolett.6b05395

17. Calusine G, Politi A et al (2014) Silicon carbide photonic crystal cavities with integrated color centers. Appl Phys Lett 105:011123. https://doi.org/10.1063/1.4890083

18. Wang J, Yu Z, Zhang X et al (2017) Efficient generation of an array of single silicon-vacancy defects in silicon carbide. Phys Rev Appl 7:064021. https://doi.org/10.1103/PhysRevApplied.7.064021

19. Chen YC, Salter PS, Knauer S et al (2017) Laser writing of coherent colour centres in diamond. Nat Photonics 11:77–80. https://doi.org/10.1038/nphoton.2016.234

20. Wang XJ, Fang HH, Sun FW et al (2022) Laser writing of color centers. Laser Photonics Rev 16:2100029. https://doi.org/10.1002/lpor.202100029

21. Gao S, Duan Y-Z, Tian Z-N et al (2022) Laser-induced color centers in crystals. Opt Laser Technol 146:107527. https://doi.org/10.1016/j.optlastec.2021.107527

22. Yamazaki Y, Chiba Y, Sato SI et al (2020) Optically detected magnetic resonance study of 3D arrayed silicon vacancies in SiC pn diodes; proceedings of the materials science forum. Trans Tech Publ. https://doi.org/10.4028/www.scientific.net/MSF.1004.343

23. Liu Y, Chen G, Song M et al (2013) Fabrication of nitrogen vacancy color centers by femtosecond pulse laser illumination. Opt Express 21:12843–12848. https://doi.org/10.1364/OE.21.012843

24. Hadden J, Bharadwaj V, Sotillo B et al (2018) Integrated waveguides and deterministically positioned nitrogen vacancy centers in diamond created by femtosecond laser writing. Opt Lett 43:3586–3589. https://doi.org/10.1364/OL.43.003586

25. Rong Y, Cheng K, Ju Z et al (2019) Bright near-surface silicon vacancy centers in diamond fabricated by femtosecond laser ablation. Opt Lett 44:3793–3796. https://doi.org/10.1364/OL.44.003793

26. Rong Y, Ju Z, Ma Q et al (2020) Efficient generation of nitrogen vacancy centers by laser writing close to the diamond surface with a layer of silicon nanoballs. New J Phys 22:013006. https://doi.org/10.1088/1367-2630/ab6351

27. Castelletto S, Almutairi A, Kumagai K et al (2018) Photoluminescence in hexagonal silicon carbide by direct femtosecond laser writing. Opt Lett 43:6077–6080. https://doi.org/10.1364/OL.43.006077

28. Chen YC, Salter PS, Niethammer M et al (2019) Laser writing of scalable single color centers in silicon carbide. Nano Lett 19:2377–2383. https://doi.org/10.1021/acs.nanolett.8b05070

29. Castelletto S, Maksimovic J, Katkus T et al (2020) Color centers enabled by direct femto-second laser writing in wide bandgap semiconductors. Nanomaterials 11:72. https://doi.org/10.3390/nano11010072

30. Castelletto S, Johnson BC, Boretti A (2020) Visible and infrared photoluminescence in hexagonal silicon carbide by direct femtosecond laser writing. IOP Conf Ser Mater Sci Eng 840:012010. https://doi.org/10.1088/1757-899X/840/1/012010

31. Hain TC, Fuchs F, Soltamov VA et al (2014) Excitation and recombination dynamics of vacancy-related spin centers in silicon carbide. J Appl Phys 115:133508. https://doi.org/10.1063/1.4870456

32. Sharma S, Mandal V, Ramakrishna S et al (2018) Numerical simulation of melt hydrodynamics induced hole blockage in Quasi-CW fiber laser micro-drilling of TiAl6V4. J Mater Process Technol 262:131–148. https://doi.org/10.1016/j.jmatprotec.2018.06.038

33. Gattass RR, Mazur E (2008) Femtosecond laser micromachining in transparent materials. Nat Photonics 2:219–225. https://doi.org/10.1038/nphoton.2008.47

34. Sörman E, Son N, Chen W et al (2000) Silicon vacancy related defect in 4H and 6H SiC. Phys Rev B 61:2613. https://doi.org/10.1103/PhysRevB.61.2613

35. Nivas JJ, He S, Song Z et al (2017) Femtosecond laser surface structuring of silicon with Gaussian and optical vortex beams. Appl Surf Sci 418:565–571. https://doi.org/10.1016/j.apsusc.2016.10.162
36. Lutey AH, Gemini L, Romoli L et al (2018) Towards laser-textured antibacterial surfaces. Sci Rep 8:1–10. https://doi.org/10.1038/s41598-018-28454-2
37. Chen J, Wan C, Zhan Q (2018) Vectorial optical fields: recent advances and future prospects. Sci Bull 63:54–74. https://doi.org/10.1016/j.scib.2017.12.014

Zhanqi Zhou, State Key Laboratory of Precision Measuring Technology and Instruments, School of Precision Instruments and Opto-Electronics Engineering, Tianjin University, China. Mr. Zhou is studying for Master degree. His research interests include the preparation of silicon carbide color centers by femtosecond laser, and Raman and fluorescence spectrum characterization.

Zongwei Xu, Professor, State Key Laboratory of Precision Measuring Technology & Instruments, Laboratory of Micro/Nano Manufacturing Technology, Tianjin University, China. His research interests include defect engineering in wide band gap semiconductor, micro/nanofabrication using focused ion beam and femtosecond laser, Raman and fluorescence spectrum, etc.
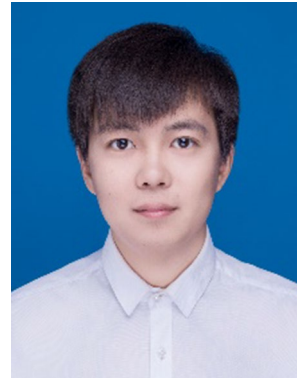
Ying Song, State Key Laboratory of Precision Measuring Technology and Instruments, School of Precision Instruments and Opto-Electronics Engineering, Tianjin University, China. Ms. Song is studying for PhD degree. Her research interests include preparation of silicon carbide color centers by ion-implantation, three-dimensional Raman and photoluminescence spectral characterization, and model of spectral depth profiling.

depth analysis model.

Changkun Shi, State Key Laboratory of Precision Measuring Technology and Instruments, School of Precision Instrument and Opto-Electronic Engineering, Tianjin University China. Mr. Shi is studying for PhD degree. His research interests include femtosecond laser processing and control of diamond NV color center, including femtosecond laser-induced graphitization damage of diamond, femtosecond laser preparation of diamond NV color center microstructure, and multi-spectral

Kun Zhang, State Key Laboratory of Precision Measuring Technology and Instruments, School of Precision Instruments and Opto-Electronics Engineering, Tianjin University, China. Mr. Zhang is studying for PhD degree. His research interests include ultrafast femtosecond laser processing, Raman spectroscopy, fluorescence spectroscopy and other technologies in the ultra-wide band gap semiconductor material gallium oxide application research.

Bing Dong, State Key Laboratory of Precision Measuring Technology and Instruments, School of Precision Instrument and Opto-Electronics Engineering, Tianjin University, China. Mr. Dong is studying for Doctor's degree.